Proceedings of Meetings on Acoustics

Volume 9, 2010 http://asa.aip.org

159th Meeting
Acoustical Society of America/NOISE-CON 2010
Baltimore, Maryland
19 - 23 April 2010
Session 1aBB: Biomedical Ultrasound/Bioresponse to Vibration

1aBB5. Feasibility study of superharmonic imaging using chirps

Paul Van Neer*, Mikhail G. Danilouchkine, Guillaume Matte, Marco M. Voormolen, Martin D. Verweij and Nico De Jong

***Corresponding author's address: Biomedical Engineering, Erasmus Medical Center, Dr. Molewaterplein 50, Rotterdam, 3015 GE, Zuid-Holland, Netherlands, p.vanneer@erasmusmc.nl**

Superharmonic imaging (SHI) targets a combination of the 3rd to 5th harmonics. It was proven to have certain advantages in comparison with the established imaging standards in medical utrasound. SHI enhances the spatial resolution and improves the quality of echographic images, mainly by eliminating reverberation artifacts at the chest wall. However, SHI suffers from ripple artifacts, originating from the spectral gaps in between harmonics, and degrading the temporal resolution. To solve this a chirp-based SHI protocol was employed and its characteristics investigated, i.e. point spread function (PSF). The protocol was implemented for an interleaved phased array probe (44+44 elements tuned at 1.0+3.7MHz), connected to a fully programmable ultrasound system. A linear chirp (center frequency 1MHz; bandwidth 40%) was used for excitation. To obtain the PSF, the RF traces were recorded at focus along the lateral axis and convolved with the decoding signal. This was computed using KZK simulations. A PSF comparison between a superharmonic chirp and the 3rd-harmonic of a 2.5-cycle Gaussian apodized sinus burst at 1MHz showed a decrease in axial pulse length of 46% at -6dB and 32% at the -20dB level in favor of SHI. Chirp based SHI is virtually free of ripple artifacts and therefore feasible.

Published by the Acoustical Society of America through the American Institute of Physics

 [DOI: 10.1121/1.3430889]
Received 29 Mar 2010; published 28 Apr 2010

1 Introduction

Second harmonic imaging is currently the de-facto standard in commercial echographic systems for diagnosis because of its improved resolution and contrast-to-tissue ratio. An emerging technique called superharmonic imaging (SHI) is based on a combination of multiple frequency components generated during the propagation of sound in tissue [1]. This combination of third to fifth harmonic has the potential to further enhance resolution and image quality of echographic pictures. Tissue SHI efficiently suppresses near-field artifacts, reverberations, and off-axis artifacts in addition to the enhanced lateral and axial resolution. The resulting images showed more details than those produced by second harmonic imaging [2].
In spite of the apparent advantages of SHI, there exists a fundamental problem associated with this method. The bandwidth of contemporary electrically tuned transducers is limited. If a pulse with limited bandwidth propagates nonlinearly in a thermoviscous medium, the resulting distorted pulse will show distinct troughs in its frequency spectrum. These troughs between the harmonics lead to ripples in the point spread function (PSF), which give rise to ghost reflections along the direction of the wave propagation in practical imaging situations.
In previous work we introduced a dual pulse method to solve the ripple issue and showed its feasibility for phased array transducers [3, 4]. The imaging protocol is based on the transmission of two pulses with the second pulse of slightly different frequency. The echoes produced by each transmission pulse are summed to create an image. The methodology produced good results, but it does have a few drawbacks. Firstly, it is based on transmitting two pulses per A-line and thus the maximum attainable frame rate is reduced by a factor of two - quite a compromise to make when imaging fast moving structures such as heart valves. Secondly, the total amount of energy transmitted into the tissue is limited. It was shown in previous work that an optimum exists between the method's ability to suppress the ripples and the length of the transmitted pulses [4]. Thus, the time-bandwidth product of the signals involved in this method is low. To improve the time-bandwidth product coded excitation could be used, which has been shown to improve the SNR by the time-bandwidth product [5]. The improved SNR leads to an increased penetration depth. This is especially useful for higher harmonic imaging, since the signal amplitudes of the higher harmonics are generally low.

In this work we employ a chirp protocol for SHI without sacrificing the acquisition speed. Its characteristics in terms of point spread functions (PSF) are investigated. The PSF used here combines the convolution of the electrical excitation (the pulsing scheme), the transmit transfer function and the spatial impulse response with the effects of nonlinear propagation and postprocessing.

2 The chirp protocol

The chirp protocol is based on coded excitation. It is based on the transmission of a pulse train with certain properties (a code). In reception the pulse train is compressed using a decoding filter to obtain an image. The first report on coded excitation in medical literature dates back to 1979 [6]. Since then a sizable volume of literature has been dedicated to imaging using coded excitation - an excellent overview is given by Misardis et al. [5, 7]. Among the codes investigated were chirps [8], orthogonal Golay codes [9] and binary sequences [10]. Recently, coded excitation using linear chirps was also used for second harmonic imaging of ultrasound contrast agents [11].
The chirp protocol for SHI consists of transmitting a frequency modulated signal and receiving the third to fifth harmonic. The recorded echo is compressed using a decoding signal. Linear chirps were used because of their higher SNR gain at large imaging depths relative to pulsed excitation compared to the SNR gain reported for nonlinear chirps and Golay codes [5]. The filtered superharmonic band of the on-axis pressure signal in focus computed with the KZK method was used for decoding.

3 Materials and methods

3.1 Experimental setup

The experimental setup consisted of a water-filled tank featuring a hydrophone (diameter 0.2 mm, Precision Acoustics, Dorchester, UK) mounted in an xyz-system. A special dual frequency transducer [12] was mounted in the tank's sidewall. The elements of the low frequency subarray were excited by linear 0.95 MHz chirps with a -6 dB bandwidth of 40%, amplitude 24 V and length 15 μs. The excitation signals were produced by a multi channel programmable

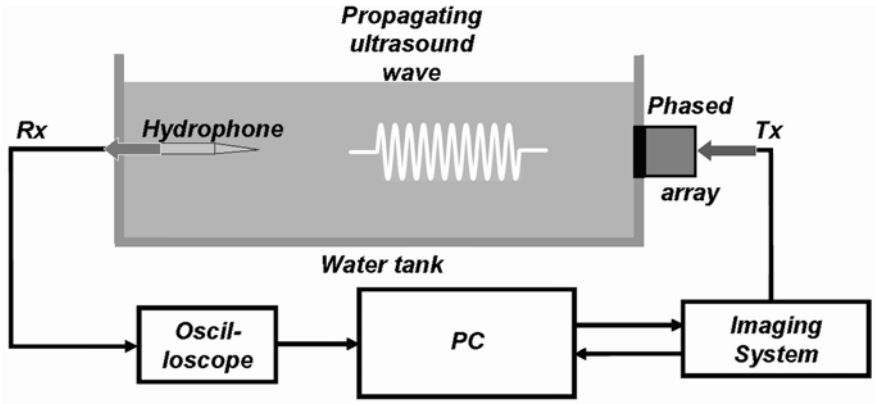

Figure 1: The experimental setup.

ultrasound system (OPEN system, Lecoeur Electronique, Chuelles, France, first reported in [13]). The signals received by the hydrophone were digitized by an oscilloscope (9400A, Lecroy, Geneva, Switzerland) with a sampling frequency of 100 MHz and transferred to a computer for further processing. The experimental setup is shown in Fig. 1.

3.2 KZK simulations

The decoding pulse was generated using simulations based on the KZK equation. The KZK equation was solved in the time domain. The nonlinearity and absorption terms were solved using the numerical methods developed by Lee et al. [14, 15]. The diffraction term was solved in the near-field using an implicit backward finite difference method and in the far field using an alternating direction implicit method. The first method is more effective in damping numerical oscillations and the latter method is more accurate allowing for larger step sizes [16]. The algorithm was implemented in the C and Matlab languages. The simulations were performed in full 3D. The low frequency subarray of the dual frequency array was used as the source: the subarray consisted of 44 elements with size 16 mm x 0.2 mm and pitch 0.5 mm [12]. The subarray was modeled as a rectangular aperture of 16 x 22 mm. The transmitted pressure was scaled to take into account the kerf between the elements. Lateral and elevation foci at 6 cm were implemented to model the elevation lens and the electronic focusing. As the input for the simulations a voltage chirp similar to the one used for the experiments was used. The voltage chirp was converted to the output pressure pulse of the low frequency subarray using the transmit transfer function [12]. The effect of the electrical impedance of the transmitter circuits was neglected as the electrical impedance the arbitrary waveform generator outputs (5 Ω) was low compared to the electrical impedance of the transducer elements (minimum magnitude of tuned impedance 100 Ω). Both the normalized chirp produced by the AWGs and the normalized chirp transmitted by the transducer are shown in Fig. 2.

4 Results

In Fig. 3 both the measured (dashed gray line) and the simulated (solid black line) on-axis pressure signals are shown. The data presented in the figure clearly shows the similarity between both pulses allowing for the use of the simulated signal for decoding of the experimental signals.

Fig. 4 shows the decoded superharmonic chirp PSF. The result presented in the figure shows a smooth and distinct peak with low compression artifacts. The obtained SNR is $\sim$35 dB.

Fig. 5 details the normalized axial intensities of the third and superharmonic components. The dual pulse superharmonic profile was obtained using the optimal settings as reported by Matte et al. [3] and van Neer et al. [4] and was obtained using Gaussian apodized 2.5 cycle sine bursts with amplitude 60 V. This was also the case for the single pulse superharmonic and third harmonic profiles. The superharmonic chirp profile was obtained using a 40% chirp with a 0.95 MHz center frequency and length 15 μs. From the figure, we see that the superharmonic chirp profile is reasonably smooth but does contain minor ripples. The axial lengths at the -6 dB level are 0.88 mm, 0.81 mm, 2.3 mm and 2.5 mm for the single pulse, optimal dual pulse and chirp superharmonic components and for the third harmonic component respectively. At the -20 dB level the axial lengths increase to 4.7 mm, 3.3 mm, 4.4 mm and 5.3

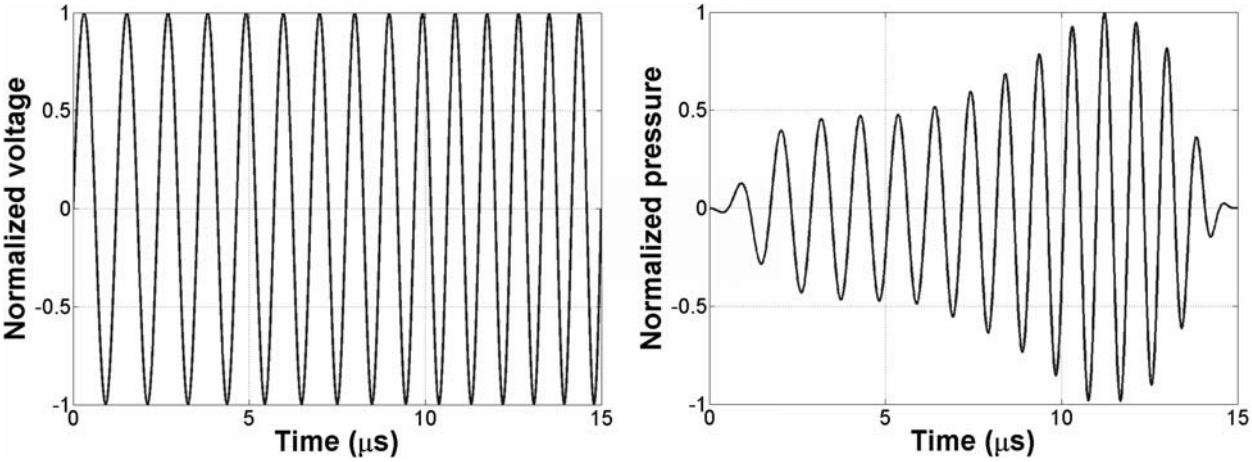

Figure 2: On the left the normalized chirp produced by the AWGs of the OPEN system. On the right the actual normalized chirp transmitted by the transducer, calculated using the transfer function.

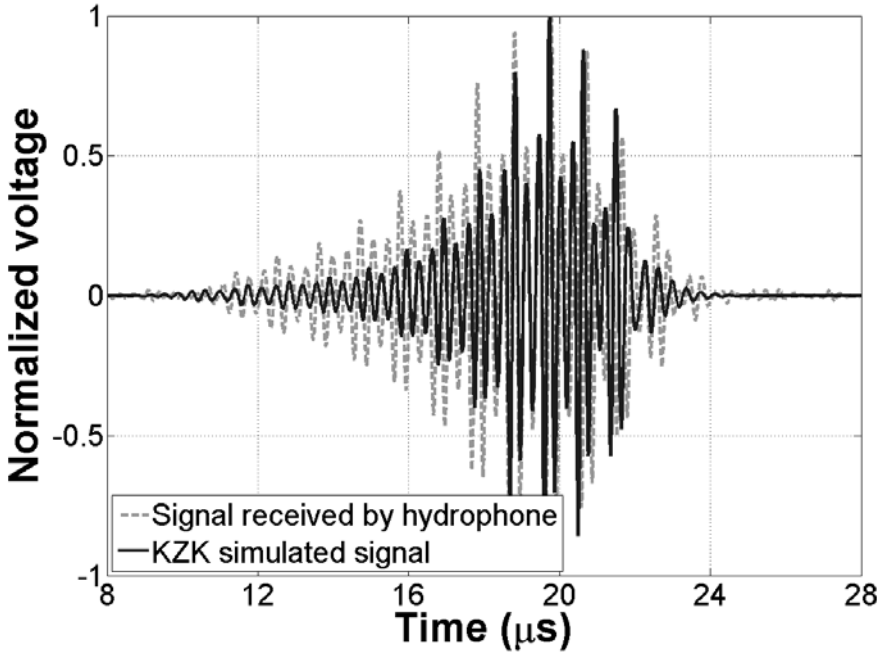

Figure 3: The on-axis pressure signal at focus. The dashed gray line displays the experimentally obtained data, the solid black line shows the KZK simulated signal.

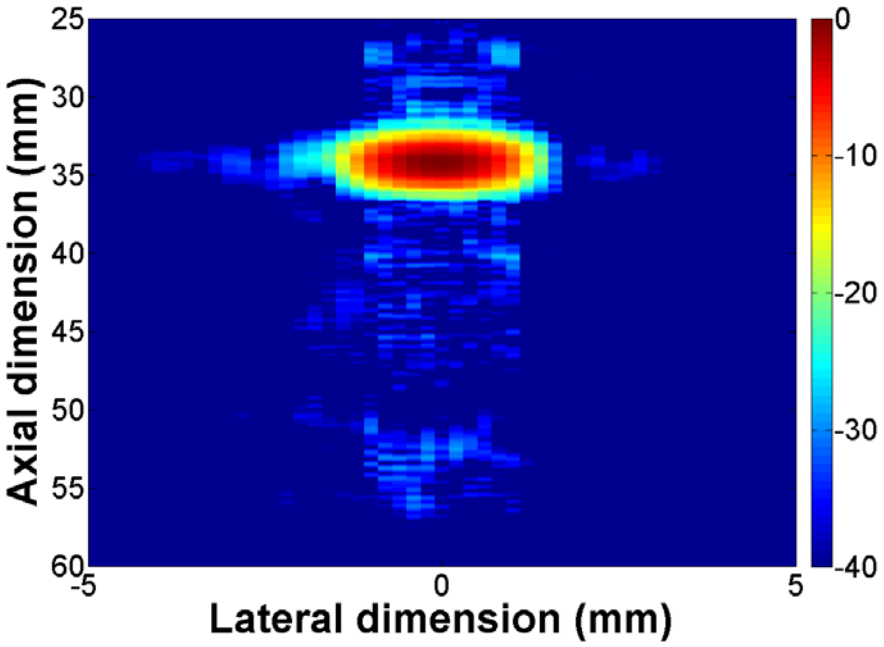

Figure 4: Decoded superharmonic chirp PSF. The relative intensity is color coded using a dynamic range of 40 dB. The transmitted signal was a 40% chirp with a 0.95 MHz center frequency and length 15 μs.

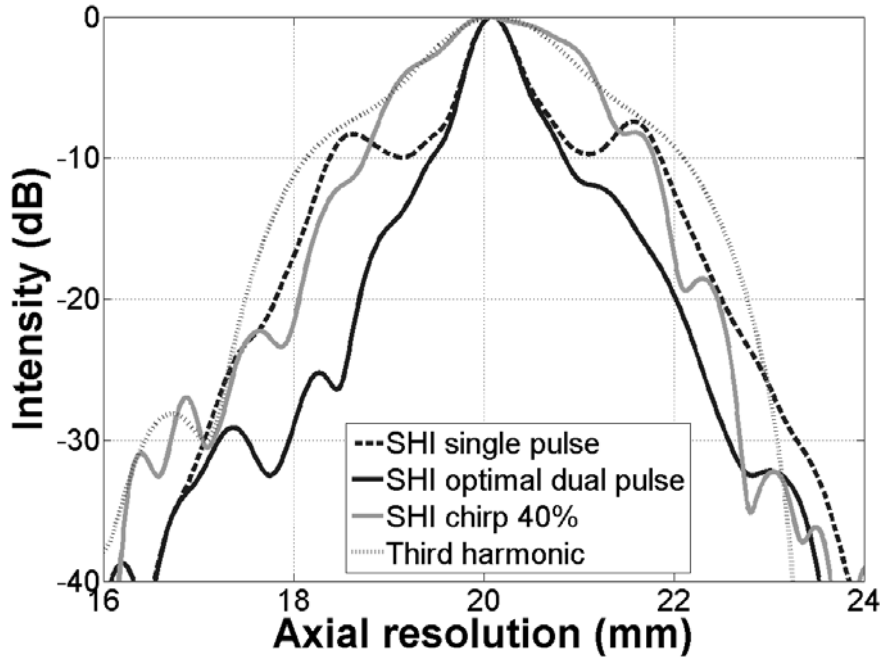

Figure 5: The normalized axial intensity profiles for the third harmonic and various superharmonic methods. The third harmonic, the optimal dual pulse [4] and single pulse superharmonic profiles are obtained using 2.5 cycle Gaussian apodized sine bursts with amplitude 60 V. The superharmonic chirp intensity profile was obtained using a 40% chirp with a 0.95 MHz center frequency and length 15 μs.

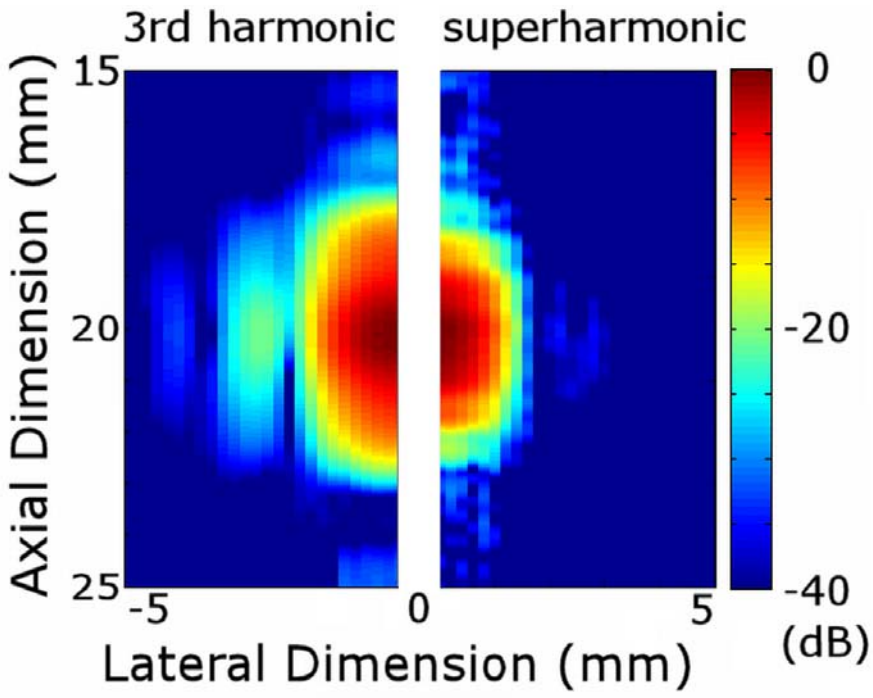

Figure 6: Comparison of the 3rd harmonic PSF obtained using 2.5 cycle transmissions (left panel) and the superharmonic chirp PSF (right panel). The relative intensity is color coded using a dynamic range of 40 dB. The third harmonic was obtained by exciting the transducer using a Gaussian apodized 2.5 cycle sine burst with amplitude 60 V.

mm respectively.
Fig. 6 displays the third harmonic PSF obtained using a 2.5 cycle Gaussian apodized sine burst on the left and the superharmonic chirp PSF on the right using a dynamic range of 40 dB. The superharmonic chirp lateral beam widths at -6 dB and -20 dB were 1.8 mm and 3 mm respectively, whereas for the third harmonic these were 2.2 mm and 3.4 mm respectively. The axial beam widths at -6 dB and -20 dB were 2.3 mm and 4.4 mm respectively for dual pulse SHI and 2.5 mm and 5.3 mm for the third harmonic.

5 Discussion

The superharmonic PSF produced by the chirp protocol is smooth and almost completely free of ripples. However, as can be seen in Fig. 3, the decoding signal can still be improved - especially at the start of the signal there are significant differences between the experimentally recorded signal and the KZK simulated signal. The amplitude differences are likely caused by nonnegligible circuit effects and the phase differences are caused by the phase transfer functions of the circuitry and the transducer.
The relative increase in the axial resolution obtained using the superharmonic chirp protocol amounts to 8% at the -6 dB level and 17% at the -20 dB level compared to the third harmonic. Whereas the relative increase in the lateral resolution obtained using the superharmonic chirp protocol is 18% and 17% at the -6 dB and -20 dB levels respectively compared to the third harmonic. If the axial resolution of the chirp superharmonic protocol is compared to the dual pulse superharmonic method reported previously [3, 4], we find a 65% decrease in resolution at the -6 dB level and a 25 % decrease at the -20 dB level. The lateral resolution produced by the superharmonic chirp method is equal to the lateral resolution of the dual pulse method at the -6 dB level and 12% higher at the -20 dB level. The intensity of the superharmonics is equally high (or higher) for the chirp excitation compared to the short burst excitation, but at 40% of the excitation voltage. Comparing the chirp and dual pulse protocols, there is a trade-off between the achievable resolution and the number of transmitted pulses per A-line. However, both imaging schemes produce a considerably better resolution than the third harmonic. It is expected that these resolutions will deteriorate somewhat in *in-vivo* situations, due to the imperfectness of the generated decoding signal (chirp method) and the influence of

tissue attenuation (dual pulse method).

6 Conclusion

The PSFs produced by the superharmonic chirp protocol are virtually free from ripple artifacts and have increased spatial resolution compared to the third harmonic. However, the spatial resolution is lower compared to the dual pulse superharmonic method [4]. Thus there exists a trade-off between the attainable spatial resolution and the frame rate in superharmonic imaging.

Acknowledgements The financial support of the Dutch Foundation for Technical Sciences is greatly appreciated.

References

[1] A. Bouakaz, S. Frigstad, F. ten Cate, and N. de Jong, "Super harmonic imaging: a new imaging technique for improved contrast detection," *Ultrasound Med. Biol.*, vol. 28, no. 1, pp. 59–68, 2002.

[2] A. Bouakaz and N. de Jong, "Native tissue imaging at superharmonic frequencies," *IEEE Trans. Ultrason. Ferroelectr. Freq. Control*, vol. 50, no. 5, pp. 496–506, 2003.

[3] G. Matte, P. van Neer, J. Borsboom, M. Verweij, and N. de Jong, "A new frequency compounding technique for super harmonic imaging," in *Proc. IEEE Ultrasonic Symp.* New York, NY: IEEE, 2008, pp. 357–360.

[4] P. van Neer, M. Danilouchkine, G. Matte, M. Verweij, and N. de Jong, "Dual pulse frequency compounded super harmonic imaging for phased array transducers," in *Proc. IEEE Ultrasonic Symp.*, Rome, Italy, 2009, pp. –.

[5] T. Misardis and J. Jensen, "Use of modulated excitation signals in medical ultrasound. part i: basic concepts and expected benefits," *IEEE Trans. Ultrason. Ferroelectr. Freq. Control*, vol. 52, no. 2, pp. 177–191, 2005.

[6] Y. Takeuchi, "An investigation of a spread energy method for medical ultrasound systems - part one: theory and investigation," *Ultrasonics*, vol. 17, no. 4, pp. 175–182, 1979.

[7] T. Misardis and J. Jensen, "Use of modulated excitation signals in medical ultrasound. part ii: design and performance for medical imaging applications," *IEEE Trans. Ultrason. Ferroelectr. Freq. Control*, vol. 52, no. 2, pp. 192–207, 2005.

[8] M. Pollakowski and H. Ermert, "Chirp signal matching and signal power optimization in pulse-echo mode ultrasonic nondestructive testing," *IEEE Trans. Ultrason. Ferrorelect. Freq. Control*, vol. 41, no. 5, pp. 655–659, 1994.

[9] R. Chiao and L. Thomas, "Synthetic transmit aperture imaging using orthogonal golay coded excitation," in *Proc. IEEE Ultrasonics Symp.*, 2000, pp. 1677–1680.

[10] J. Shen and E. Ebbini, "A new coded-excitation ultrasound imaging system - part i: basic principles," *IEEE Trans. Ultrason. Ferroelect. Freq. Control*, vol. 43, no. 1, pp. 131–140, 1996.

[11] J. Borsboom, C. Chin, and N. de Jong, "Nonlinear coded excitation method for ultrasound contrast imaging," *Ultrasound Med. Biol.*, vol. 29, pp. 277–284, 2003.

[12] P. van Neer, G. Matte, M. Danilouchkine, C. Prins, F. van den Adel, and N. de Jong, "Super harmonic imaging: development of an interleaved phased array transducer," *IEEE Trans. Ultrason. Ferroelectr. Freq. Control*, vol. 57, no. 2, pp. 455–468, 2010.

[13] F. Vignon, J.-F. Aubry, M. Tanter, A. Margoum, M.Fink, and J. Lecoeur, "Dual-arrays brain imaging prototype: Experimental in vitro results," in *Proc. IEEE Ultrasonic Symp.*, Rotterdam, the Netherlands, 2005, pp. 504–507.

[14] Y. Lee, "Numerical solution of the kzk equation for pulsed finite amplitude sound beams in thermoviscous fluids." PhD-thesis, The University of Texas, 1993.

[15] Y. Lee and M. Hamilton, "Time-domain modeling of pulsed finite-amplitude sound beams," *J. Acoust. Soc. Am.*, vol. 97, no. 2, pp. 906–917, 1995.

[16] M. Voormolen, "3d harmonic echocardiography," Ph.D. dissertation, Erasmus University Rotterdam, 2007.